Moore, Steven I.; Ruppert, Michael G.; Yong, Yuen Kuan. "Design and analysis of piezoelectric cantilevers with enhanced higher eigenmodes for atomic force microscopy", Published Proceedings of the 2017 IEEE International Conference on Advanced Intelligent Mechatronics (AIM) (Munich, Germany 3-7 July, 2017) p. 719-724. (2017)

Available from: http://dx.doi.org/10.1109/AIM.2017.8014102

Design and Analysis of Piezoelectric Cantilevers with Enhanced Higher Eigenmodes for Atomic Force Microscopy

Steven I. Moore[1], Michael G. Ruppert[1] and Yuen K. Yong[1]

***Abstract*— Atomic force microscope (AFM) cantilevers with integrated actuation and sensing provide several distinct advantages over conventional cantilever instrumentation such as clean frequency responses, the possibility of down-scaling and parallelization to cantilever arrays as well as the absence of optical interferences. However, for multifrequency AFM techniques involving higher eigenmodes of the cantilever, optimization of the transducer location and layout has to be taken into account. This work proposes multiple integrated piezoelectric regions on the cantilever which maximize the deflection of the cantilever and the piezoelectric charge response for a given higher eigenmode based on the spatial strain distribution. Finite element analysis is performed to find the optimal transducer topology and experimental results are presented which highlight an actuation gain improvement up to 42 dB on the third mode and sensor sensitivity improvement up to 38 dB on the second mode.**

***Index Terms*— Design/control of MEMS-nano devices; Micro-Electro-Mechanical Systems; Applications of nano technology**

I. INTRODUCTION

The atomic force microscope [1] has established itself as a sophisticated instrument to study a variety of samples, ranging from soft materials, like DNA, cells, proteins and polymers to stiff materials such as silicon and graphite [2].

At the heart of the AFM, a microcantilever with a sharp tip interrogates the surface of a sample to create a 3D image of its topography. Moreover, dynamic modes where the cantilever is actively driven at its first resonance frequency, enables gentle interaction forces [3], specifically for the investigation of biologically-relevant samples. For these modes, the observed change in the amplitude of the cantilever's oscillation signal is commonly used to provide the feedback signal for the z-axis control loop; the controller output is used to map the topography of the sample.

In order to go beyond the study of the sample's topography, excitation and detection with a number of frequencies was shown to lead to a significant improvement for nanomechanical characterization [4]. Specifically, higher order eigenmodes of the cantilever provide enhanced imaging properties such as a higher modal stiffness and a faster response time [5] and when used in multimodal imaging were shown to be more sensitive to material properties [6]–[8].

The need for clean cantilever actuation becomes apparent since additional resonances introduced by the commonly used piezoelectric stack actuator at the base of the cantilever yields highly distorted frequency responses. This fact makes higher mode identification and analysis exceedingly difficult. As such, a number of integrated actuation methods including photothermal [9], resistive thermal [10] or via a piezoelectric layer [11] have been successfully employed.

The optical beam deflection method [12] is still considered the widely used standard for measuring the cantilever oscillation mostly owing to its low noise characteristics [13]. However, the method comes with practical limitations such as frequent laser alignment and fundamental limitations in terms of the minimum laser spot size which requires minimum cantilever dimensions [14]. Therefore, integrated sensing methodologies such as piezoresistive [15]–[17] and piezoelectric [18]–[20] techniques are of great interest largely due to their smaller footprints and advantages in scalability [21].

Piezoelectric transduction seems particularly promising due to the inherent capability to serve as both an actuator and sensor even with a single active layer [22]–[24]. However, previously proposed cantilever designs only employ a single piezoelectric layer [25]–[27] which is not optimized to be used for sensing higher order modes. While it was recently shown that these modes can still be sensed with appropriate signal conditioning [28], their observability depends strongly on the location and layout of the piezoelectric layer.

This work outlines the design of a piezoelectric layer topology for AFM cantilevers in order to maximize the actuator gain and sensor sensitivity for higher order eigenmodes. Mindlin plate theory and finite element analysis is employed from which the spatial distribution of the strain for a given higher mode is determined. As a result, the piezoelectric layer is split into multiple isolated areas such that the response from regions with equal polarity are constructively combined to maximize the actuator gain and sensor output for higher order flexural and torsional eigenmodes.

II. MODAL ANALYSIS OF THE PIEZOELECTRIC CANTILEVER

The fundamental cantilever geometry analyzed in this work is shown in Fig. 1. The stepped rectangular design has the benefit of closely spaced higher eigenmodes compared to rectangular cantilever shapes [29] as well as amplified higher mode deflections [30]. A finite element (FE) model is developed for modal analysis using Mindlin plate theory to model the cantilever [31]. The piezoelectric layer is assumed to be thin compared to the silicon layer.

When the cantilever is deflected, a charge is produced, which can be calculated as the integral of the electric

*This work was supported by the Australian Research Council

[1]The authors are with the School of Electrical Engineering and Computing, The University of Newcastle, Callaghan, NSW 2308, Australia steven.i.moore@uon.edu.au, michael.ruppert@newcastle.edu.au, yuenkuan.yong@newcastle.edu.au

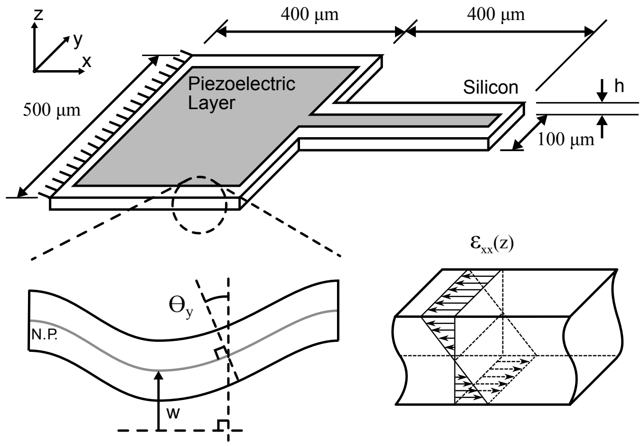

Fig. 1. Schematic of the basic cantilever shape and dimensions. The zoomed in section of the plate shows the out-of-plane deflection w and the rotation of the normal of the cantilever's neutral plane (N.P.) about the y-axis θ_y as well as the resulting in-plane strain in the x-direction.

displacement D_3 [32]

$$q(t) = \iint_A D_3 \, \mathrm{d}A, \tag{1}$$

where A is the area of the piezoelectric layer. The electrodes are uniformly distributed on both sides of the piezoelectric layer, the piezoelectric material is homogeneous and only poled along the z-axis. Therefore, the electric displacement in the piezoelectric material with only non-zero components can be stated as [32], [33]

$$D_3 = d_{31}\varepsilon_{xx} + d_{32}\varepsilon_{yy}, \tag{2}$$

where $d_{31} = d_{32} = d_p$ are the piezoelectric coefficients and $\varepsilon_{xx/yy}$ are the surface strains along the x- and y-axis, respectively (compare Fig. 1).

The modal analysis based on the FE model provides the solutions in terms of the out-of-plane deflection $w(x, y, t)$ as well as the rotations of the normal of the cantilever's neutral plane around the x-axis $\theta_x(x, y, t)$ and y-axis $\theta_y(x, y, t)$, respectively. Since the piezoelectric layer is assumed to be thin compared to the silicon layer, the response of the piezoelectric transducer is proportional to the surface strains of the cantilever which are stated as a function of the rotations as [34]

$$\begin{aligned} \varepsilon_{xx} &= \frac{h}{2}\frac{\partial \theta_y}{\partial x}, \\ \varepsilon_{yy} &= -\frac{h}{2}\frac{\partial \theta_x}{\partial y}. \end{aligned} \tag{3}$$

Substituting (3) and (2) into (1) yields

$$q(t) = \frac{dh}{2}\int_y \int_x \frac{\partial \theta_y}{\partial x} - \frac{\partial \theta_x}{\partial y} \, \mathrm{d}x \, \mathrm{d}y. \tag{4}$$

A common approach to solve for the rotations θ_x and θ_y is to assume that the solution can be represented by separable space and time functions representing the mode shapes $\phi_x(x, y)$ and $\phi_y(x, y)$ and modal coordinates $u(t)$ [35]:

$$\begin{aligned} \theta_x(x, y, t) &= u(t)\phi_x(x, y), \\ \theta_y(x, y, t) &= u(t)\phi_y(x, y). \end{aligned} \tag{5}$$

When the area from (1) is restricted to the area A_e of a single rectangular element from the FE mesh, the modal analysis calculates the rotations θ_x^e and θ_y^e at the four nodes of the element. Then, the mode shapes over an element are

$$\begin{aligned} \phi_x^e(x, y) &= N^T(x, y)\theta_x^e, \\ \phi_y^e(x, y) &= N^T(x, y)\theta_y^e \end{aligned} \tag{6}$$

where $N(x, y)$ are the shape functions [31], [34]

$$N(x, y) = \begin{bmatrix} \frac{1}{4}(1 - \frac{x}{a})(1 - \frac{y}{b}) \\ \frac{1}{4}(1 + \frac{x}{a})(1 - \frac{y}{b}) \\ \frac{1}{4}(1 + \frac{x}{a})(1 + \frac{y}{b}) \\ \frac{1}{4}(1 - \frac{x}{a})(1 + \frac{y}{b}) \end{bmatrix} \tag{7}$$

with the dimensions of a rectangular element being $2a \times 2b$ and its origin placed at the center. Substituting the mode shapes into (4), the charge response of the piezoelectric transducer over a single FE element is found to be

$$q^e(t) = u(t)\frac{d_p h}{2}\iint_{A_e} \frac{\partial N}{\partial y}\theta_x^e - \frac{\partial N}{\partial x}\theta_y^e \, \mathrm{d}x \, \mathrm{d}y. \tag{8}$$

Since the shape functions are quadratic in x and y, the derivatives are linear. Hence, the integral can be evaluated exactly using Gaussian quadrature at the midpoint of the element. Evaluating q^e for each element of a piezoelectric transducer and summing over the entire cantilever provides the overall charge response for a given eigenmode.

III. Multimodal Cantilever Designs

First, modal analysis is performed on the cantilever geometry shown in Fig. 1 using the finite element method. For the FE analysis, an elastic modulus of $169\mathrm{GPa}$, density of $2500\mathrm{kgm}^{-3}$ and Poisson's ratio of 0.29 were assumed as the material properties of the silicon. The resulting simulated mode shapes of the first four modes of the cantilever are shown in Section 2 (a)-(d). The modal frequencies are $38.3\mathrm{kHz}$, $119\mathrm{kHz}$, $176\mathrm{kHz}$, and $342\mathrm{kHz}$.

Second, the piezoelectric layer configuration for each mode is found by calculating the integral in (8) for every element in the mesh. If the sign of the integral for two neighboring elements is the same, their responses add constructively otherwise destructively. Consequently, the piezoelectric layer is split into a positive and a negative transducer shown in Fig. 2(e)-(h) which are actuated and sensed with opposite polarities. For flexural modes, the strain ε_{xx} dominates the charge response whereas the strain ε_{yy} is insignificant over most parts of the cantilever. However, near the cantilever tip the opposite occurs which causes the small electrodes seen in Fig. 2 (e),(f) and (h).

The piezoelectric cantilever designs were fabricated using the PiezoMUMPs fabrication process by MEMSCAP [36]

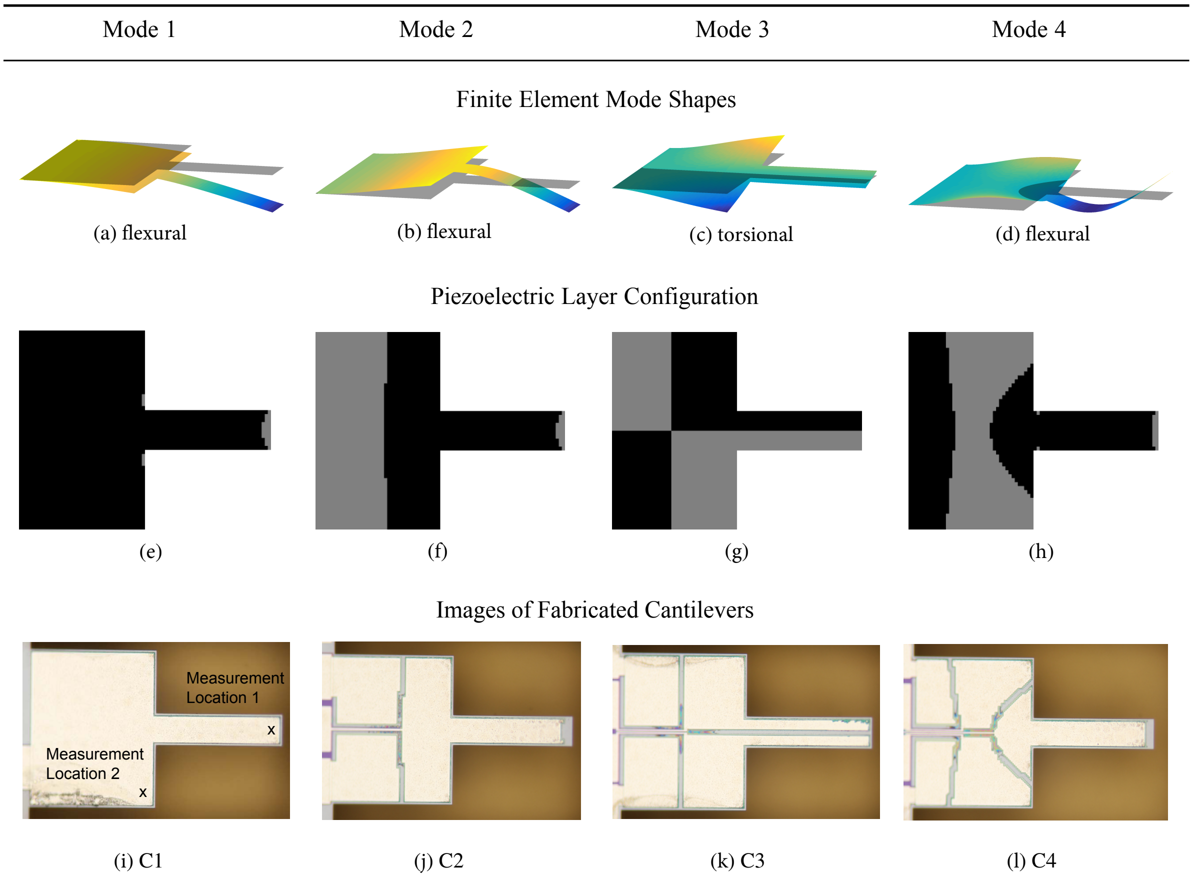

Fig. 2. (a)-(d) The first four mode shapes of the cantilever from the FE model. (e)-(f) The piezoelectric arrangement to maximize the response of the transducer to each mode. The gray electrodes induce a charge in the opposite polarity to the black electrodes. (m)-(p) The fabricated cantilever designs.

and are shown in Fig. 2 (i)-(l). The thickness of the single-crystal-silicon device layer is $10\,\mu\mathrm{m}$ with a $0.5\mu\mathrm{m}$ layer of AlN and a $1\mu\mathrm{m}$ layer of Aluminum for electrical connections. A limitation of the PiezoMUMPs process is the inability to fabricate tips, preventing the demonstration of AFM imaging using the proposed designs. The authors are currently working on post-fabricating tips using focused ion beam deposition [37], [38].

Since the mechanical modeling neglects the piezoelectric material and in order to account for fabrication tolerances, the design routine was executed with large parameter variations. It was found that the mode shapes and thus the shape of the piezoelectric transducers is invariant to variations in the density of $1000-4000\mathrm{kgm}^{-3}$, elasticities of $120-280\mathrm{GPa}$, for Poisson's ratio of $0.2-0.4$ and for a silicon thickness of $8-15\mu\mathrm{m}$.

IV. Instrumentation

A. Instrumentation Design

The microfabrication process used results in a common terminal between all piezoelectric transducers [36]. In order to achieve electrical isolation, the common node has to be grounded and the actuation and sensing circuits have to be applied to a grounded load. This is achieved with a grounded load charge sensor as shown in Fig. 3 where the voltage across each piezoelectric area serves as actuation. The driving op-amp maintains the input signal V_i across each piezoelectric layer and the charge generated by the strain dependent voltage source V_p is measured across a reference capacitor C_s with a differential amplifier. A FET input op-amp (TI, OPA656) is used to buffer the piezoelectric transducer. The component values of the circuit elements used are $C_s = 10\mathrm{pF}$, $R_s = 1\mathrm{M}\Omega$ and $R_p = 10\mathrm{M}\Omega$.

B. Instrumentation Modeling

A voltage applied to the electrodes of a piezoelectric layer results in a bending moment causing the cantilever to deflect. The transfer function from actuation voltage $V_i(s)$ to tip displacement $D(s)$ can be described by a sum of n second order modes [32]

$$G_{dv}(s) = \frac{D(s)}{V_i(s)} = \sum_{i=1}^{n} G_{dv}^{i}(s) = \sum_{i=1}^{n} \frac{\alpha_i \omega_i^2}{s^2 + \frac{\omega_i}{Q_i} s + \omega_i^2}, \quad (9)$$

where each second order term is characterized in terms of the resonance frequency ω_i, quality factor Q_i, and gain α_i. When the cantilever deflects, the strain on the surface of the piezoelectric transducer induces a charge on its electrodes which can be modeled as a strain dependent voltage source

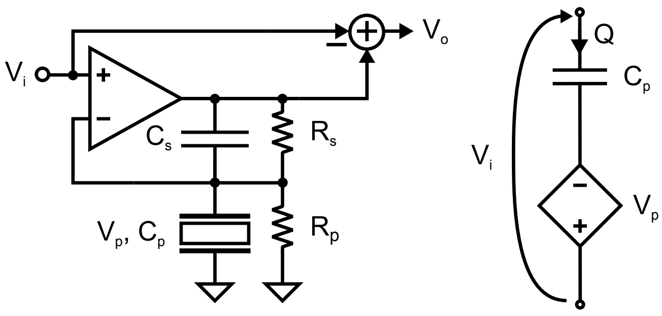

Fig. 3. The instrumentation circuit for the grounded load charge sensing arrangement and the electrical model of a piezoelectric layer.

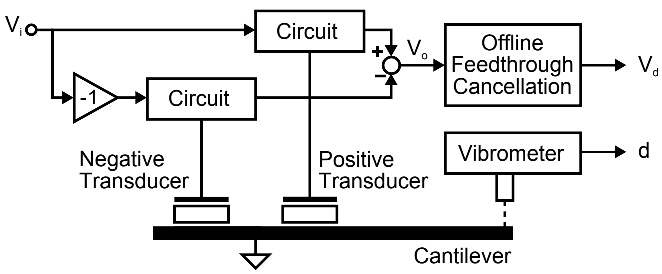

Fig. 4. The experimental setup to characterize the cantilever designs.

$V_p(s)$ in series with the piezoelectric capacitance C_p as shown in Fig. 3. The transfer function from the actuation voltage to the piezoelectric voltage is [32]

$$G_{vv}(s) = \frac{V_p(s)}{V_i(s)} = \sum_{i=1}^{n} \delta_i G_{dv}^i(s). \tag{10}$$

and the transfer function from actuation voltage to charge $Q(s)$ can be found to be [28]

$$G_{qv}(s) = \frac{Q(s)}{V_i(s)} = C_p + C_p G_{vv}(s). \tag{11}$$

Notice, that there are two charge terms in this transfer function, one associated with feedthrough from the actuation voltage and one associated with the motion of the cantilever. As such, the output of the self-sensing instrumentation circuit is

$$V_o(s) = \frac{R_s(sC_pR_p+1)}{R_p(sC_sR_s+1)}V_i(s) + \frac{sC_pR_s}{sC_sR_s+1}V_p(s). \tag{12}$$

The resistance R_p and R_s are chosen such that the pole at $1/2\pi R_s C_s$ and zero at $1/2\pi R_p C_p$ are much lower than the resonance frequencies of the cantilever. Then for frequencies in the pass band, the output voltage can be simplified to

$$V_o(s) = \frac{C_p}{C_s}V_i(s) + \frac{C_p}{C_s}V_p(s). \tag{13}$$

Since generally $V_i(s) \gg V_p(s)$, the feedthrough component almost entirely conceals the motional component. Therefore, in order to used the piezoelectric transducer for self-sensing the feedthrough has to be canceled in real-time to maximize the dynamic range of the sensor. This can be achieved with feedforward compensators implemented on Field Programmable Analog Arrays as prototyping systems [23] or in analog [28]. Here, the feedthrough is estimated and removed offline to demonstrate the sensor sensitivity increase of the fabricated tip-less cantilevers.

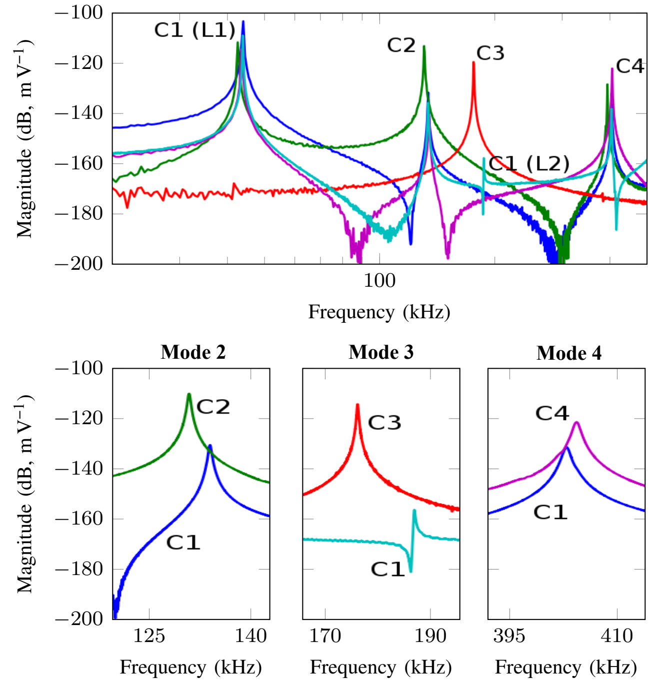

Fig. 5. Magnitude frequency responses of the cantilevers C1-C4 from input voltage V_i to displacement d measured with the laser Doppler vibrometer. The flexural modes of C1, C2, and C4 are measured at location 1 (L1) while the torsional mode M3 is measured at location 2 (L2) (compare Fig. 2(i)).

TABLE I

ACTUATION GAIN OF THE REFERENCE CANTILEVER C1 AND THE OPTIMIZED CANTILEVERS C2-C4: MAGNITUDE OF DISPLACEMENT RESPONSES ($V_i \longrightarrow d$).

Mode	Ref. Gain [μm/V]	Opt. Gain [μm/V]	Δ Gain [dB]
M1	(C1) 16.97	-	-
M2	(C1) 2.968×10^{-1}	(C2) 3.125	20.45
M3	(C1) 1.522×10^{-2}	(C3) 1.927	42.05
M4	(C1) 2.667×10^{-1}	(C4) 8.475×10^{-1}	10.04

V. EXPERIMENTAL RESULTS

A. Experimental setup

The experimental setup in order to characterize the cantilever designs is shown in Fig. 4. The displacement responses from V_i to d for each mode are measured with a laser Doppler vibrometer (Polytec MSA-400) at two locations which are shown in Fig. 2 (i). Two differentially driven instrumentation circuits are connected to the positive and negative transducer and their respective responses are combined constructively to yield V_o. The feedthrough component is removed offline by fitting a third order transfer function to the measured response over a small frequency band around each resonance. This model accounts for a second order mechanical system according to (9) and a first

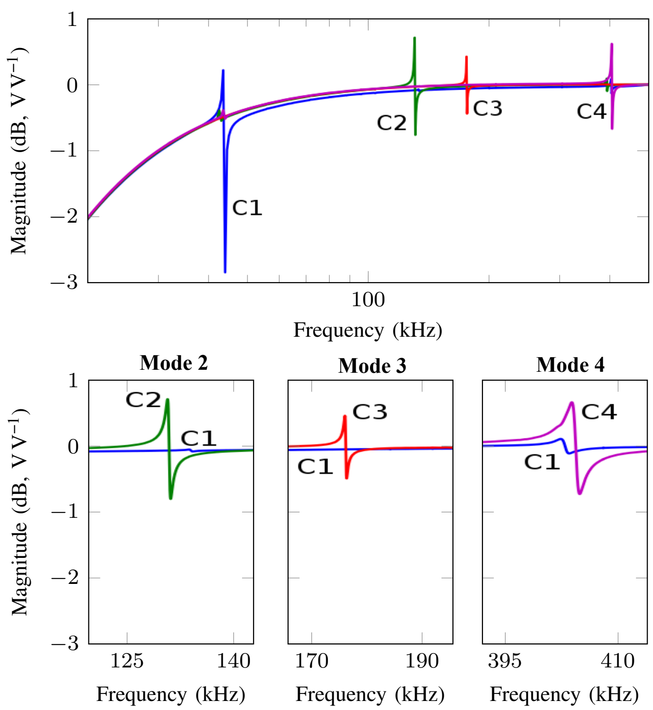

Fig. 6. Magnitude frequency responses from V_i to output voltage V_o, C1-C4 are shifted to 0dB to account for different C_p values of each cantilever.

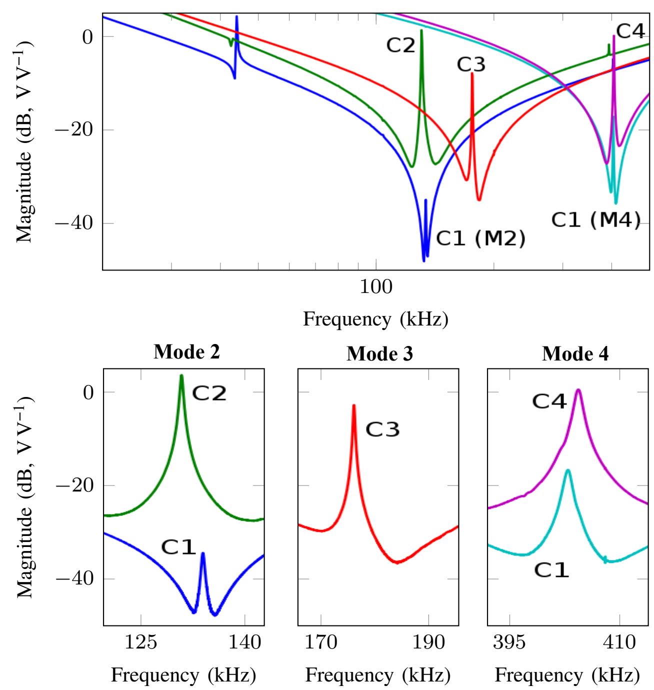

Fig. 7. Magnitude frequency responses of the cantilevers C1-C4 from V_i to sensor output V_d after feedthrough cancellation.

TABLE II
PARAMETERS OF THE IDENTIFIED TRANSFER FUNCTIONS.

	C_p/C_s	Q_i	f_i [kHz]	$\delta_i\alpha_i$
C1 (M1)	5.433	408.6	43.92	1.395×10^{-3}
C1 (M2)	5.716	316.6	133.5	9.630×10^{-6}
C1 (M4)	5.756	358.9	402.9	7.074×10^{-5}
C2 (M2)	8.698	309.0	130.7	5.545×10^{-4}
C3 (M3)	6.718	608.9	175.9	1.761×10^{-4}
C4 (M4)	6.728	381.0	404.3	4.144×10^{-4}

TABLE III
SENSITIVITIES OF THE REFERENCE CANTILEVER C1 AND THE OPTIMIZED CANTILEVERS C2-C4: MAGNITUDE OF SENSOR RESPONSES WITHOUT FEEDTHROUGH ($V_i \longrightarrow V_d$).

Mode	Ref. Gain $[VV^{-1}]$	Opt. Gain $[VV^{-1}]$	Δ Gain [dB]
M1	(C1) 3.265	-	-
M2	(C1) 1.910×10^{-2}	(C2) 1.514	37.98
M3	-	(C3) 7.247×10^{-1}	-
M4	(C1) 1.471×10^{-1}	(C4) 1.061	17.16

order feedthrough system according to (12). The identified feedthrough is subtracted from the measurements to produce the sensor response without feedthrough, i.e. from V_i to V_d.

B. Discussion

The improvement in actuation gain at the resonance frequencies of the optimized piezoelectric layer topologies is evaluated from the measured frequency responses from V_i to d shown in Fig. 5; the magnitudes at each mode are stated in Table I. From the response, the resonance frequencies of the first four modes of the reference C1 cantilever are found to be 44.02kHz, 133.7kHz, 186.8kHz and 402.9kHz, respectively. Fabrication tolerances and the negligence of the piezoelectric layer in the FE analysis account for the frequency differences compared to the FE model in Section III. From Fig. 5 it can be seen that compared to the reference cantilever C1, the actuation gain is increased by 20.45dB for C2 at mode 2, 42.05dB for C3 at mode 3 and 10.04dB for C4 at mode 4.

The increase in sensor sensitivity using the proposed self-sensing instrumentation is assessed by measuring the frequency response from input voltage V_i to sensor output voltage V_o and is shown in Fig. 6. For the unoptimized reference cantilever C1 and due to substantial feedthrough, the higher order modes M2 and M4 are barely noticeable and M3 is entirely unobservable. In contrast, the optimized higher mode cantilevers C2-C4 clearly show the resonances.

The gain in sensitivity is attained by fitting the third order transfer functions (13) to the response in Fig. 6 around the resonances; the parameters are stated in Table II. The discrepancy from the ideal second order response is due to residual feedthrough originating from unmodeled parasitic capacitances in the MEMS device and read-out circuit. From the fit, the feedthrough C_p/C_s is identified (compare Table II) and subtracted to yield the magnitude responses from input voltage V_i to sensor output V_d shown in Fig. 7. Compared to C1, the sensitivity is increased by 37.98dB for C2 at mode 2 and 17.16dB for C4 at mode 4 (compare Table III). Note, that C3 enables measurement of the torsional mode, which was unobservable for C1.

VI. CONCLUSIONS

AFM cantilevers with integrated piezoelectric layers are versatile transducers due to their self-actuating and self-sensing capability. However, for applications in multifrequency AFM, the electrode layout has to be optimized in order to properly excite and sense higher order eigenmodes of the cantilever. In this work, we provide a systematic way of splitting up the piezoelectric layer into several transducers, whose individual responses are constructively combined to yield increased actuator gain and sensor sensitivity on higher modes. The required instrumentation for the resulting three terminal piezoelectric device is realized with a grounded load charge sensor. The experimental results highlight an improvement in actuation gain of up to $42\,\mathrm{dB}$ on the third mode, sensitivity increase of up to $38\,\mathrm{dB}$ on the second mode and strong observation of torsional modes compared to an unoptimized electrode layout. Future work will focus on the fabrication of tips for high-resolution multimodal AFM.

REFERENCES

[1] G. Binnig, C. F. Quate, and C. Gerber, "Atomic force microscope," *Phys. Rev. Lett.*, vol. 56, no. 9, pp. 930–933, 1986.

[2] S. Morita, F. J. Giessibl, and R. Wiesendanger, *Noncontact Atomic Force Microscopy*. Springer-Verlag Berlin Heidelberg, 2009.

[3] R. Garcia and R. Prez, "Dynamic atomic force microscopy methods," *Surface Science Reports*, vol. 47, no. 6-8, pp. 197–301, 2002.

[4] R. Garcia and E. T. Herruzo, "The emergence of multifrequency force microscopy," *Nature nanotechnology*, vol. 7, no. 4, pp. 217–226, 2012.

[5] M. G. Ruppert and S. O. R. Moheimani, "Multimode Q control in tapping-mode AFM: Enabling imaging on higher flexural eigenmodes," *IEEE Trans. Contr. Syst. Technol.*, vol. 24, no. 4, pp. 1149–1159, July 2016.

[6] T. R. Rodriguez and R. García, "Compositional mapping of surfaces in atomic force microscopy by excitation of the second normal mode of the microcantilever," *Appl. Phys. Lett.*, vol. 84, no. 3, pp. 449–451, 2004.

[7] N. F. Martínez, S. Patil, J. R. Lozano, and R. García, "Enhanced compositional sensitivity in atomic force microscopy by the excitation of the first two flexural modes," *Appl. Phys. Lett.*, vol. 89, no. 15, p. 153115, 2006.

[8] E. T. Herruzo, A. P. Perrino, and R. Garcia, "Fast nanomechanical spectroscopy of soft matter," *Nature communications*, vol. 5, no. 3126, pp. 1–8, 2014.

[9] N. Umeda, S. Ishizaki, and H. Uwai, "Scanning attractive force microscope using photothermal vibration," *Journal of Vacuum Science & Technology B*, vol. 9, no. 2, pp. 1318–1322, 1991.

[10] G. E. Fantner, D. J. Burns, A. M. Belcher, I. W. Rangelow, and K. Youcef-Toumi, "DMCMN: In Depth Characterization and Control of AFM Cantilevers With Integrated Sensing and Actuation," *Journal of Dynamic Systems Measurement and Control-Transactions of the Asme*, vol. 131, no. 6, pp. 061 104–061 104–13, 2009.

[11] S. Akamine, T. Albrecht, M. Zdeblick, and C. Quate, "A planar process for microfabrication of a scanning tunneling microscope," *Sensors and Actuators A: Physical*, vol. 23, no. 1, pp. 964 – 970, 1990.

[12] G. Meyer and N. M. Amer, "Novel optical approach to atomic force microscopy," *Appl. Phys. Lett.*, vol. 53, no. 12, pp. 1045–1047, 1988.

[13] T. Fukuma, M. Kimura, K. Kobayashi, K. Matsushige, and H. Yamada, "Development of low noise cantilever deflection sensor for multienvironment frequency-modulation atomic force microscopy," *Rev. Sci. Instrum.*, vol. 76, no. 5, 2005.

[14] R. Kassies, K. O. van der Werf, M. L. Bennink, and C. Otto, "Removing interference and optical feedback artifacts in atomic force microscopy measurements by application of high frequency laser current modulation," *Rev. Sci. Instrum.*, vol. 75, no. 3, pp. 689–693, 2004.

[15] M. Tortonese, R. C. Barrett, and C. F. Quate, "Atomic resolution with an atomic force microscope using piezoresistive detection," *Appl. Phys. Lett.*, vol. 62, no. 8, pp. 834–836, 1993.

[16] R. Linnemann, T. Gotszalk, L. Hadjiiski, and I. Rangelow, "Characterization of a cantilever with an integrated deflection sensor," *Thin Solid Films*, vol. 264, no. 2, pp. 159 – 164, 1995.

[17] R. Jumpertz, A. Hart, O. Ohlsson, F. Saurenbach, and J. Schelten, "Piezoresistive sensors on afm cantilevers with atomic resolution," *Microelectronic Engineering*, vol. 41, pp. 441 – 444, 1998.

[18] J. Tansock and C. Williams, "Force measurement with a piezoelectric cantilever in a scanning force microscope," *Ultramicroscopy*, vol. 42, pp. 1464 – 1469, 1992.

[19] T. Itoh and T. Suga, "Development of a force sensor for atomic force microscopy using piezoelectric thin films," *Nanotechnology*, vol. 4, no. 4, p. 218, 1993.

[20] P.-F. Indermühle, G. Schürmann, G.-A. Racine, and N. de Rooij, "Fabrication and characterization of cantilevers with integrated sharp tips and piezoelectric elements for actuation and detection for parallel AFM applications," *Sensors and Actuators A: Physical*, vol. 60, no. 1-3, pp. 186 – 190, 1997.

[21] M. Dukic, J. D. Adams, and G. E. Fantner, "Piezoresistive AFM cantilevers surpassing standard optical beam deflection in low noise topography imaging," *Scientific Reports*, vol. 5, no. 16393, pp. 1–11, 2015.

[22] J. Adams, L. Manning, B. Rogers, M. Jones, and S. Minne, "Self-sensing tapping mode atomic force microscopy," *Sensors and Actuators A: Physical*, vol. 121, no. 1, pp. 262 – 266, 2005.

[23] M. G. Ruppert and S. O. R. Moheimani, "A novel self-sensing technique for tapping-mode atomic force microscopy," *Rev. Sci. Instrum.*, vol. 84, no. 12, p. , 2013.

[24] ——, "Novel reciprocal self-sensing techniques for tapping-mode atomic force microscopy," in *Proc. 19th IFAC World Congress*. Cape Town, South Africa: IFAC, 7 2014.

[25] C. Lee, T. Itoh, and T. Suga, "Self-excited piezoelectric PZT microcantilevers for dynamic SFM - with inherent sensing and actuating capabilities," *Sensors and Actuators A: Physical*, vol. 72, no. 2, pp. 179 – 188, 1999.

[26] H. Quenzer, U. Drechsler, A. Sebastian, S. Marauska, B. Wagner, and M. Despont, "Fabrication of conducting AFM cantilevers with aln-based piezoelectric actuators," *Procedia Engineering*, vol. 25, pp. 665 – 668, 2011.

[27] A. Sebastian, N. Shamsudhin, H. Rothuizen, U. Drechsler, W. W. Koelmans, H. Bhaskaran, H. J. Quenzer, B. Wagner, and M. Despont, "Note: Micro-cantilevers with aln actuators and ptsi tips for multi-frequency atomic force microscopy," *Rev. Sci. Instrum.*, vol. 83, no. 9, p. , 2012.

[28] M. G. Ruppert and S. O. R. Moheimani, "High-bandwidth multimode self-sensing in bimodal atomic force microscopy," *Beilstein J. Nanotechnol.*, vol. 7, pp. 284–295, 2016.

[29] S. Sadewasser, G. Villanueva, and J. A. Plaza, "Special cantilever geometry for the access of higher oscillation modes in atomic force microscopy," *Appl. Phys. Lett.*, vol. 89, no. 3, p. 033106, 2006.

[30] A. Salehi-Khojin, S. Bashash, and N. Jalili, "Modeling and experimental vibration analysis of nanomechanical cantilever active probes," *Journal of Micromechanics and Microengineering*, vol. 18, no. 8, p. 085008, 2008.

[31] M. Petyt, *Introduction to Finite Element Vibration Analysis*. Cambridge University Press, 1998.

[32] S. O. Moheimani and A. J. Fleming, *Piezoelectric Transducers for Vibration Control and Damping*. Springer, 2006.

[33] K. Jian and M. I. Friswell, "Designing distributed modal sensors for plate structures using finite element analysis," *Mechanical Systems and Signal Processing*, vol. 20, no. 8, pp. 2290–2304, 2006.

[34] S. Quek and G. Liu, *Finite Element Method: A Practical Course*. Elsevier Science, 2003.

[35] C. W. De Silva, *Vibration - Fundamentals and Practice*. CRC Press, 2000.

[36] A. Cowen, G. Hames, K. Glukh, and B. Hardy, *PiezoMUMPs Design Handbook*, 1st ed. MEMSCAP Inc., 2014.

[37] I. Utke, P. Hoffmann, and J. Melngailis, "Gas-assisted focused electron beam and ion beam processing and fabrication," *Journal of Vacuum Science & Technology B: Microelectronics and Nanometer Structures*, vol. 26, no. 4, p. 1197, 2008.

[38] M. G. Ruppert, A. G. Fowler, M. Maroufi, and S. O. R. Moheimani, "On-chip dynamic mode atomic force microscopy: A silicon-on-insulator MEMS approach," *IEEE J. Microelectromech. Syst.*, vol. 26, no. 1, pp. 215–225, Feb 2017.